DOI: 10.21062/mft.2023.035  http://www.journalmt.com

# Effect on Surface Properties of H13 Mold Steel Cladding Layer by Scanning Strategy

Changlong Zhao (0000-0001-7778-3494), Junbao Yang (0000-0002-4958-6546), Ming Li (0000-0003-4202-0256), Qinxiang Zhao (0000-0002-6584-0196), Hongnan Ma (0000-0003-2906-2486), Xiaoyu Jia (0000-0003-4843-9947) Haifeng Zhang* (0000-0001-9522-1006)
College of mechanical and vehicle engineering, Changchun University, Changchun, Jilin Province, China. E-mail: zhao19790204@126.com; 2547025748@qq.com

**Laser cladding technology is used to clad the surface layer of H13 mold steel with Ni60A metal powder coating to solve the failure problem. The study used JMatPro software to extract and fit the thermophysical property parameters of the substrate and the clad material, and then used ANSYS APDL software to qualitatively analyze the distribution of melt pool morphology, nodal temperature versus time course curve and residual stress magnitude during the laser cladding process. Based on the results of the minimum residual stress in the cladding, reasonable scan paths were derived for the preparation of metal coatings on the surface layer of the die steel. The results show that the maximum peak temperature of the cladding process is 2515° C using short path scanning. The cladding layer can form a good metallurgical bond with the substrate at this temperature, with a stress of 406.68 MPa in the scanning direction and 284.45 MPa perpendicular to the scanning direction, which is significantly smaller than the residual stresses of other scanning methods. The residual stress values for the different strategies are from largest to smallest: spiral scan, block scan, long path scan, and short path scan. The results of this study provide theoretical guidance for the selection of paths during cladding processing to reduce the waste of resources and also provide new ideas for exploring the feasibility of metallurgical bonding of materials to substrates.**

**Keywords:** Laser Cladding, Numerical Simulation, Scanning Path, Residual Stress

## 1 Introduction

With the development of the manufacturing industry, the demand and use of molds are increasing. Due to the complex environment in which molds are located, they are subjected to high temperatures, alternating loads and thermal cycling for long periods of time, resulting in wear and fatigue damage, leading to their failure or even scrap [1]. The preparation of high-performance metallurgical coatings on the surface layer of mold steel by laser cladding technology can effectively improve the high-temperature resistance, wear resistance, and fatigue resistance of mold steel, thus enhancing its service life and reducing production costs [2,3].

The current limitations of testing methods and experimental costs make it difficult to obtain experimental values for the temperature of key nodes within the substrate, the centre of the melt pool, and the residual stresses within the cladding layer during processing. As a result, numerical finite element (FE) simulations are used by many researchers. The FEA method allows experimental studies of the process parameters, material composition, heat source model, and mechanical properties of laser cladding, saving a lot of human and financial resources. Ren Zhonghe et al. [4] studied the effect of laser power and scanning speed on the distribution of temperature as well as stress fields based on thermal-force indirect coupled nonlinear FE analysis. Ma L et al. [5] investigated the stress distribution in several cladding tracks and predicted the crack expansion based on this. Wu Yu et al. [6] used ABAQUS FE software to model the composite heat source, calculated the temperature and stress fields of the cladding layer, and analyzed the residual stresses under reciprocal and unidirectional scanning paths, respectively. Nusrat Tamanna et al. [7] investigated the progress of numerical simulations for different stages in the cladding process to model powder flow, melt pool and cladding properties. Some basic assumptions in current numerical models were outlined. Zhu Lida et al. [8] constructed a three-dimensional FE model of H13 steel and investigated the optimal cladding parameters such as overlap rate, scanning strategy, Z-axis increment and multi-layer stacking method. VUNDRU C et al. [9-10] developed a coupled thermal-force FE model of multilayer laser clad H13 tool steel and explored the evolution of residual stresses along the cross-section under different process conditions to determine the optimum process conditions for the mitigation of tensile residual stresses.

All of the above studies provide some guidance on the FE simulation of laser cladding. In order to investigate the effect of different scanning strategies on the scan path of the clad layer and the temperature of the surrounding characteristic points when cladding Ni60A on the surface of H13 mold steel, and also to select a suitable scanning strategy to improve the overall temperature distribution as well as the quality of the mold. In this paper, ANSYS APDL FE analysis is used to establish a computational model for single-layer multi-orbital laser cladding, and to qualitatively analyze the melt pool shape, nodal temperature variation with time course as well as the distribution of residual stresses during the cladding process, and to design an optimal scan path for the cladding process of H13 mold steel with the minimum residual stress value of the clad layer as the optimization target.

## 2 Finite element model building

### 2.1 Mathematical model building

This study used coaxial simultaneous powder-feeding laser cladding. It is assumed that the self-fusing alloy powder is in a molten state after being irradiated by the laser, the powder is heated uniformly per unit volume, and the uniform body heat source model is selected according to the characteristics of the heat source model, and its mathematical model is as follows:

$$q = \frac{\eta UI}{V} \tag{1}$$

Where:

$\eta$ …The laser melting thermal efficiency;

$U$ …The working voltage (V);

$I$ …The working current (A);

$V$ …The heat source action volume ($m^3$).

Laser cladding is a non-linear transient heat transfer process, the heat transfer methods are mainly divided into three kinds of heat conduction, heat convection, and heat radiation. The differential equation for three-dimensional transient heat transfer is obtained from Fourier's law and the law of conservation of energy as follows [11].

$$c\rho\frac{\partial T}{\partial t} = \lambda\left(\frac{\partial^2 T}{\partial x^2} + \frac{\partial^2 T}{\partial y^2} + \frac{\partial^2 T}{\partial z^2}\right) + \frac{\partial q_v}{\partial t} \tag{2}$$

Where:

$T$ …The temperature function (℃);

$t$ …The time (s);

$q_v$ …The heat source per unit volume ($W/mm^2$), there is no heat source inside the substrate during the laser melting process, so $q_v$ takes the value of zero;

$c$ …The specific heat capacity [J/(kg·℃)];

$\rho$ …The density ($kg/mm^3$);

7…The thermal conductivity [W/(m·℃)].

About the boundary conditions, during laser cladding, along with the movement of the laser spot, the formation of the surface melt pool, the heat gradually expands outwards from the spot, at this moment there is a temperature gradient difference between the substrate and the clad material, the exchange of heat by way of heat conduction, according to Fourier's law the heat conduction formula can be expressed as follows [12-13].

$$q^* = -k_{nn}\frac{dT}{dn} \tag{3}$$

Where:

$q^*$ …The heat flow density [W/ ($m^2$·K)];

$K_{nn}$ …The thermal conductivity [W/(m·°C)];

$T$ …The heat transfer surface temperature;

$n$ …The heat flow from the high temperature region to the low temperature region along the direction normal to the heat transfer surface.

Thermal convection refers to the input of laser energy to the workpiece, the temperature difference makes itself and the external medium or air to exchange heat, generally choosing to melt the surface layer for convection, available Newtonian cooling equation is expressed as follows.

$$q^* = \alpha\left(T_s - T_b\right) \tag{4}$$

Where:

$\alpha$ …The convective heat transfer coefficient ($W/m^2$);

$T_s$ …The physical surface temperature (°C);

$T_b$ …The surrounding medium temperature (°C).

### 2.2 The setting of material properties and process parameters

In this paper, Ni60A was chosen as the cladding material and H13 steel as the base material. In order to obtain reliable material properties, JMatPro software was used to observe the phases of metal precipitation at different temperatures for H13 mold steel and Ni60A alloy powder, as shown in Fig. 1.

The above diagram shows that the phase structure is influenced by temperature and alloy composition, and its thermophysical parameters change accordingly. Ignoring the latent heat for the phase change of the material and the bias of the composition during the melting process, it is considered that the internal organization of the material changes uniformly with increasing temperature during the laser cladding process. The least squares fit the data mutation points generated at a certain temperature during the calculation of certain thermophysical parameters is carried out as follows [14].

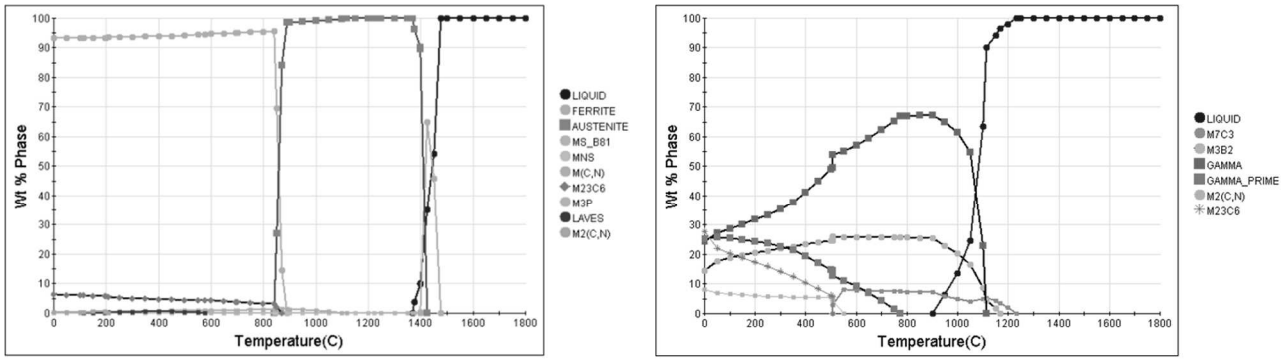


*(a) Equilibrium phase diagram* *(b) Equilibrium phase diagram of Ni60A alloy powder*

***Fig. 1*** *Temperature dependence of alloy equilibrium phase precipitation*

$$F\left(a_0,a_1,\cdots,a_m\right)=\sum_{i=1}^{n}\left[y_i-P_m(x_i)\right]^2=\min_{\Psi\in H}\sum_{i-1}^{n}\left[y_i-\psi(x_i)\right]^2$$

$$\frac{\partial F}{\partial a_j}=-2\sum_{i=1}^{n}\left[y_i-\sum_{k=0}^{m}a_k x_i^k\right]x_i^j=0\quad\left(j=0,1,\cdots,m\right) \tag{5}$$

Move the term to get:

$$\sum_{k=0}^{m}a_k\left(\sum_{i=1}^{n}x_i^{k+j}\right)=\sum_{i=1}^{n}y_i x_i^j\ \left(j=0,1,\cdots,m\right) \tag{6}$$

Interpolation of the thermophysical parameters for the H13 mold steel and Ni60A alloy powder at different temperatures, according to the temperature range of its solid-liquid phase line, determine the temperature value of the powder and the base material when the melted coating reaches 1350°C, the two metallurgical bonding, the formation of a dense coating, the value of each parameter is shown in Fig. 2.

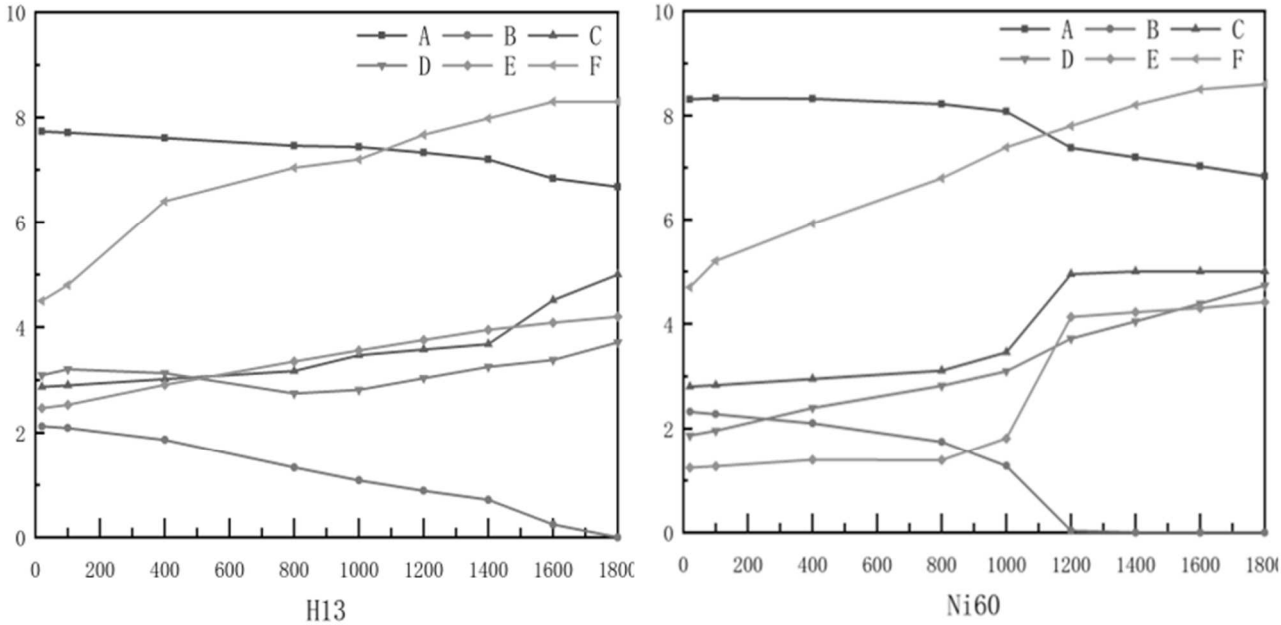


*(a) Thermo-physical parameters* *(b) Thermophysical parameters of Ni60A alloy powder*

***Fig. 2*** *Thermophysical values of materials as a function of temperature*

The parameters for laser cladding were set as follows: laser power 800 W, scanning speed 10 mm/s, spot diameter 2 mm, the effective radius of the laser source 2 mm, initial temperature 22 ° C, inter-edge conditions taking into account heat conduction and heat convection, see (3-2) and (3-3) for the specific calculation formulae, fixing method using the substrate bottom surface fixing, cooling method air-cooled. Under these process conditions, the laser cladding was numerically simulated for different scanning paths.

### 2.3 Finite element numerical models

The laser cladding substrate model size is 80mm×40mm×12mm, and the single cladding layer size is 60mm×2mm×0.8mm. According to the characteristics of laser cladding, considering the calculation time and calculation accuracy, the hexahedral mesh was divided in a sweeping way, and the mesh was densely divided near the center of the cladding, with a size of 0.5mm; the transition zone was on both sides, which is not greatly affected by the temperature, and a mesh of 2mm was chosen for the division. SOLID70 was selected for meshing, whose main features are the possibility of three-dimensional transient analysis and the conversion of temperature and structural fields [15-16]. In this paper, the indirect coupling method is used to apply and remove loads through "Element Birth and Death" in ANSYS, solving first for the temperature field and then for the structural force field. The "Element Birth and Death" principle is used to simulate the addition (or removal) of material during the actual process by controlling the "presence" (or extinction) of the corresponding cells in the cladding layer. This shows the dynamics of the powder as it is fused to the substrate, and the mesh is divided as shown in Fig. 3.

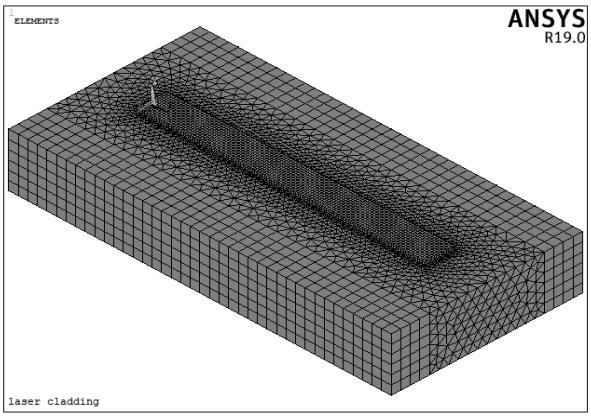


***Fig. 3*** *Finite element mesh model of single-layer three-path cladding layer*

Based on this, a single-layer multi-path laser cladding FE model with different scanning strategies was established. The substrate size was set to 60mm×12mm×32mm; The long path scan single layer length was 60mm, width was 2mm, height was 0.8mm, and 8 cladding layers were welded; The short path scan single layer size was 16mm×2mm×0.8mm, and 20 cladding layers were welded; The outward spiral scan initial single layer length, width, and height were set to 28mm, 2mm and 0.8mm, and the layer size was expanded from outward expansion. The block scanning divides the melt area into four blocks, and the length of the melt layer in the diagonal area was ensured to be equal on the model, with the dimensions of 20mm×2mm×0.8mm and 8mm×2mm×0.8mm respectively.

The physical model of laser cladding with four scanning paths is shown in Fig. 4, where Fig. a shows the long path reciprocal scanning method, with the X-axis as the scanning direction when laser cladding is formed, and the fusion paths are identified by numbers 1 to 8 from top to bottom. Path 1 was defined as the path along the X-direction, and Path 2 was the path along the Y-direction. The starting position of Path 2 is 19 mm from the left end of the cladding layer, and the starting position of Path 1 is 7 mm from the lower end of the cladding layer. Similarly, Fig. 4b, Fig. 4c, and Fig. 4d illustrate the same method as Fig. 4a. The block scanning method should be completed in the X-axis direction as a priority. To facilitate the subsequent study of the node temperature change, the intersection of Path1 and Path2 is represented by nodes P1, P2, P3, and P4, respectively. These four nodes are used to ensure that the laser beam reaches this node with the same area of the formed cladding layer and the same total heat input by different paths.

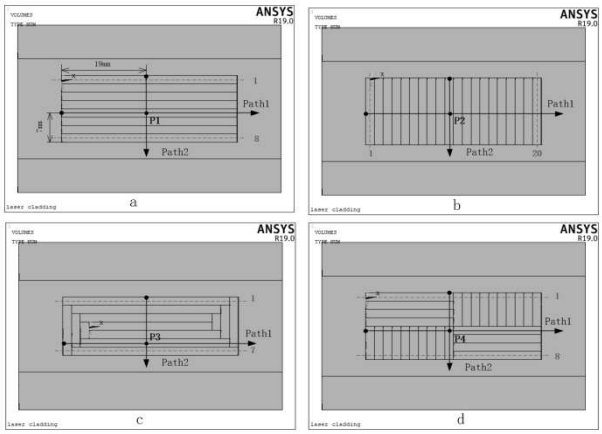


***Fig. 4*** *Physical model of laser cladding under different paths*

## 3 Analysis of numerical simulation results of temperature field

### 3.1 Analysis of the melt pool temperature field

To monitor the transient temperature and size of the melt pool under different scanning paths, the shape of the melt pool at the end of the melt path was selected for analysis. In the process of selection, it should be ensured that the effective heating time is the same for laser cladding and that the surface area after cladding is the same size. For the long path scan, the melt pool position is selected at the end of the 7th cladding layer, the short path scan is selected at the end of the 15th cladding layer, the spiral scan is selected at the outermost end of the left end, and the block scan is selected at the end of the 5th cladding layer on the lower right side, i.e. its time nodes are 13.1s, 14.9s, 12.6s, and 15.5s, respectively, and the melt pool under each path is selected as shown in Fig. 5.

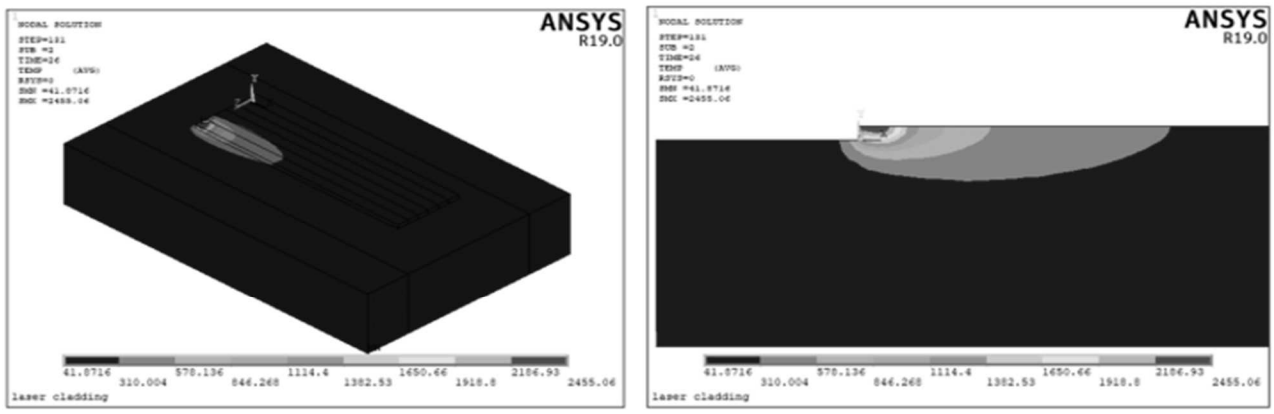


(a) t=13.1s

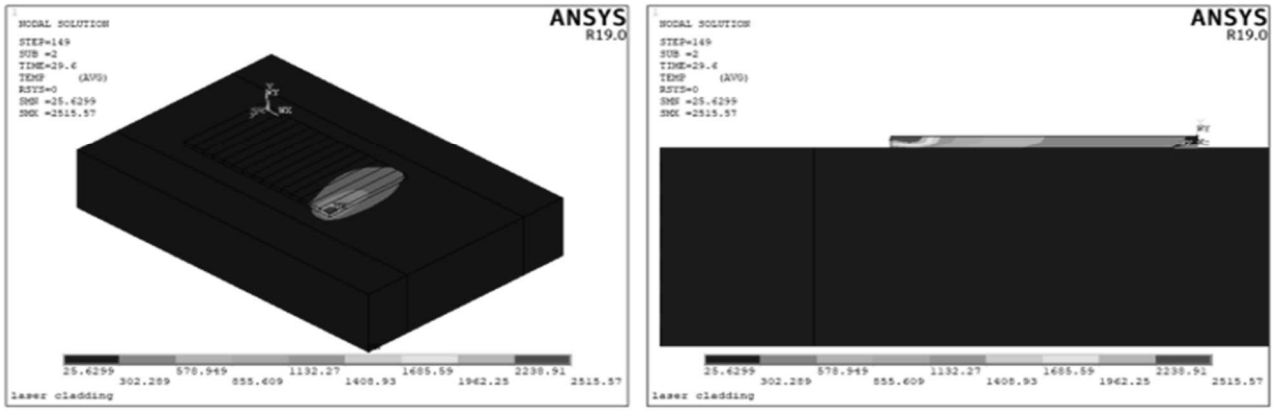


(b) t=14.9s

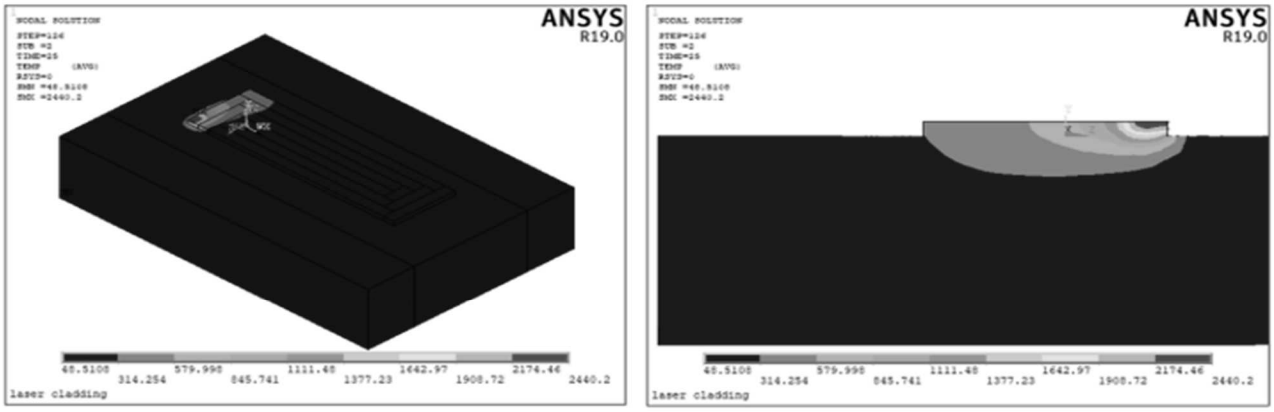


(c) t=12.6s

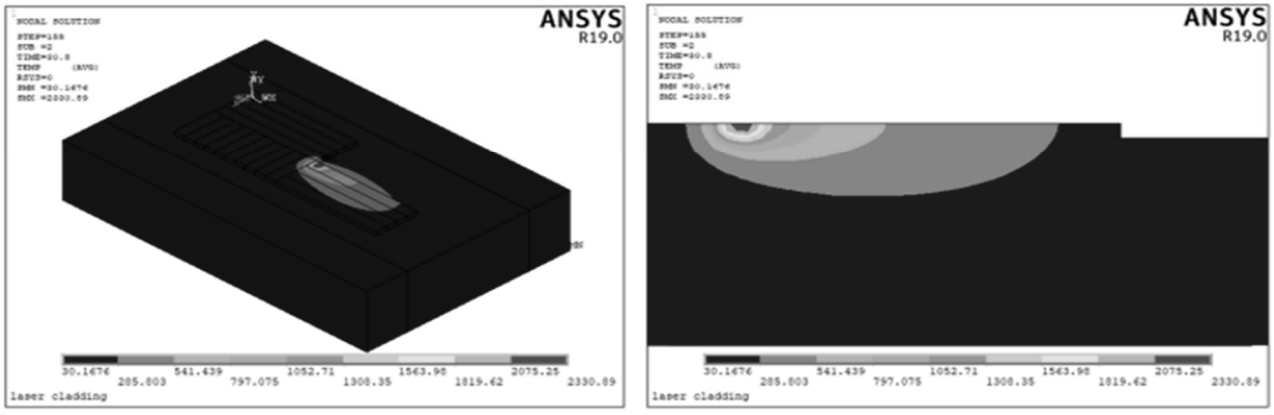


(d) t=15.5s

***Fig. 5*** *Shape of laser cladding pool with different scanning paths*

As shown in the above figures, the isotherm at the front end of the melt pool is dense during the moving process, and the end of the melt pool is trailing with a long tail, which is elliptically distributed, with the melt pool as the center, and the temperature cloud is gradually spread from the red high-temperature area to the surrounding of the substrate. In the melting process, the temperature gradient at the front end of the melt pool is significantly larger than the temperature gradient at the end, which is easy to cause large residual stress. It is mainly due to the energy input from the front-end laser, which leads to the output energy of heat conduction between the molten material and the substrate in a short time being much smaller than the input energy. The surface layer temperature can reach thousands of degrees Celsius, and the molten material at the end of the melt pool gradually changes from liquid to solid, and the heat conduction ability between liquid-solid is much smaller than that between solid, and the front-end isotherm of the melt pool is more intensive than the end isotherm under the influence of factors such as thermal radiation and convective heat transfer in the melt pool [17, 18].

Fig. 5 (a) is the long path scan, the lowest temperature of the substrate is 41.8℃ and the highest temperature of the melt pool center is 2455℃. Fig. 5 (b) is the short path scan, (c) is the spiral scan, and (d) is the block scan the lowest and highest temperatures are 25.6℃ and 2515℃; 48.5℃ and 2440℃; 30.1℃ and 2330℃ respectively. The minimum temperatures of the long path scan and spiral scan are slightly higher than the other two groups, mainly because the melting distance of the long path scan method is longer, the heat conduction time to the substrate after melting is more, and the substrate temperature has increased. When spiral scanning, the melting path gradually expands from inside to outside, and the inner melt path dissipates heat outward, with obvious heat transfer. When short path scanning, the time interval between adjacent melt paths is short. It is known from Fourier's law that the smaller the temperature gradient of the object, the slower the heat conduction, resulting in local accumulation of heat, lower temperature away from the substrate region, and higher melt pool temperature. When block scanning, the block sequence is influenced by the block sequence, which is not conducive to the accumulation of heat, and the highest melt pool temperature is the lowest. Based on the above analysis, short-path scanning is beneficial to the accumulation of heat, which can make the temperature difference in the laser cladding process smaller, while long-path scanning has a large temperature gradient.

### 3.2 Temperature-time history analysis of the surface sampling node of the cladding layer

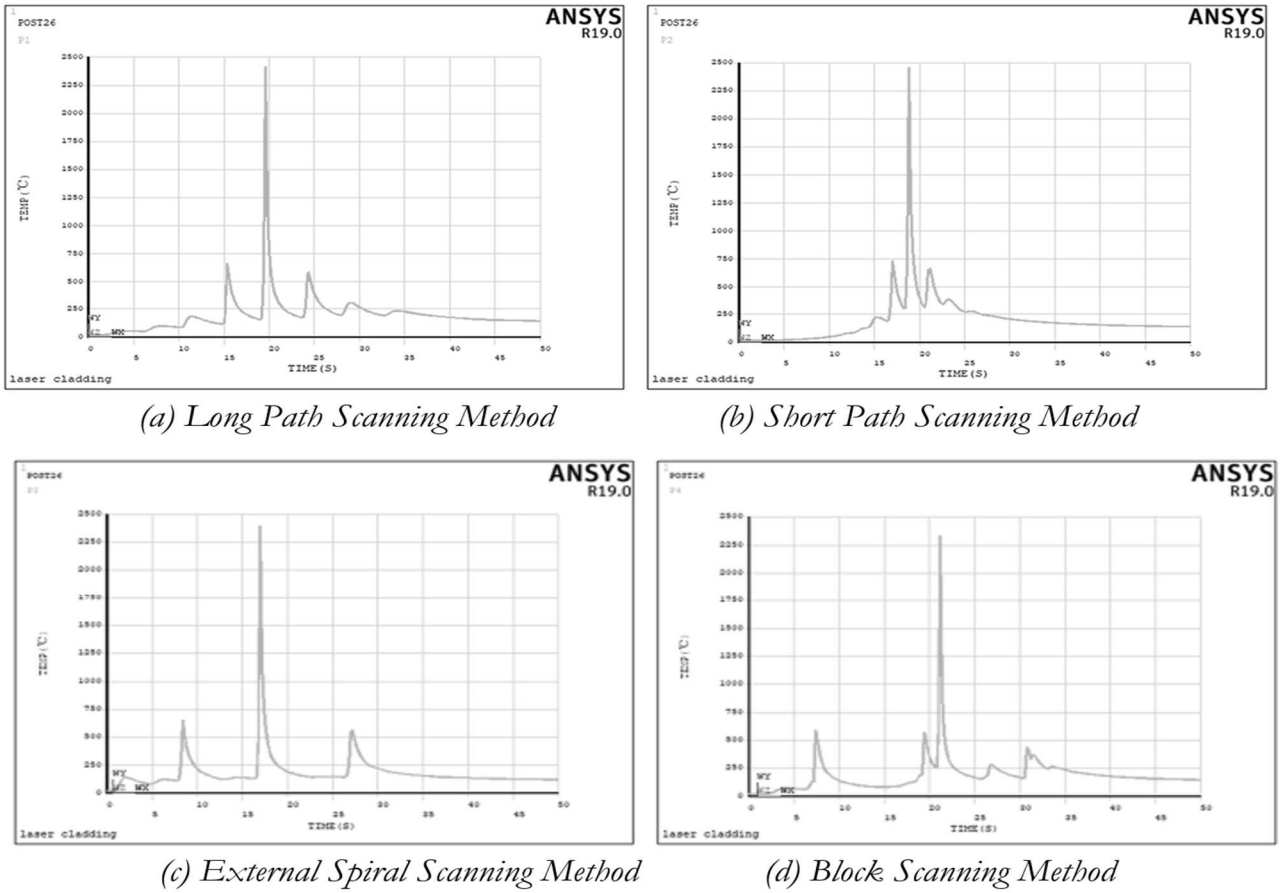


*(a) Long Path Scanning Method* *(b) Short Path Scanning Method*

*(c) External Spiral Scanning Method* *(d) Block Scanning Method*

***Fig. 6*** *Node temperature evolution with time for different scan paths*

In order to investigate the thermal influence of adjacent melt paths in different scanning methods, the intersection of paths Path1 and Path2 in each scanning strategy was chosen to be represented by points P1, P2, P3 and P4, with node numbers 4659, 3887, 1912 and 7607, respectively, and the specific selected positions can be referred to Fig. 2, where the nodes are all at the top of the melt pool, and the temperature evolution law with time is shown in Fig. 6.

The overall change trend of the top node of the melt pool under each scanning path in the figure is about the same, the whole temperature change is "saddle-shaped", the highest temperature about the center node shows symmetry, and the temperature of the node undergoes three large changes. At the initial stage, the temperature of each node was kept at room temperature of 20°C. When the laser heat source moved to the top of the node, the temperature of the node was heated up rapidly, and the temperature far exceeded the melting point of the powder material, and the temperature of the melt pool was maximized. When the node is scanned to the position directly below the next cladding layer, the node again experiences a short temperature rise due to heat transfer, and finally, the heat gradually dissipates and cools to room temperature. The maximum temperature of the node under the different scanning methods mentioned above is different, in which the melt pool temperature of spiral scanning and block scanning is lower than that of short path scanning and long path scanning as a whole, which shows that the selection of different scanning paths has an impact on the melt pool temperature and heat affected zone.

### 3.3 Analysis of the effect of scan path and slow cooling between fusion channels on node temperature

In the laser melting process, in order to simulate the laser moving to the starting position of the next melting channel after each melting channel, during which the movement of the empty stroke is carried out, two load steps without heat source are set to load after each melting channel for 0.2 s. During this period, the substrate model has no energy input and only convective heat exchange and heat conduction are carried out between the substrate and the melting layer. The data points of nodes P1, P2, P3 and P4 with time course were selected and intercepted for the melting time period from 5s to 35s, and their node variation curves are shown in Fig. 7.

Fig. 7 shows the node change law with time under four scanning paths. The node experienced three temperature changes, which can be interpreted as a preheating effect by the residual heat of the molten zone, and the cooling rate of the previous molten layer was slowed down by the heat-affected zone of the next melt path. The same node was in the heat-affected zone of the previous melt layer when the temperature increased for the first time under different scanning methods, and the temperatures were 662°C, 733° C, 652°C, and 586°C. As the laser action position changes, the heat-affected zone gradually disappears and the node temperature dropped to the lowest values of 154°C, 302°C, 125°C, and 83°C. Subsequently, the node morphology undergo a solid-liquid-solid transition. The overall trend of node temperature change in the four paths shows consistency, and the temperature curves all shows a sharp climb and rapid decline, which reflects the characteristics of laser melting with rapid cooling and heating, but the slope of the curve in the warming stage is large, which tends to produce a large temperature gradient between the melt pool and the substrate.

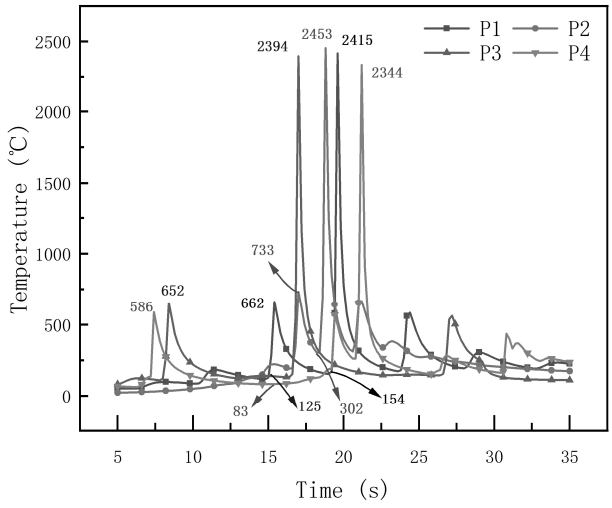


***Fig. 7*** *Node temperature evolution with time for different scan paths*

The red curve in the above figure represents the short path scan, which has the shortest time interval between the three temperature peaks, and the lowest temperature of the coating during the cladding period is 302°C, which is greater than the lowest temperature of the other scanning paths. This is because the contact time between the melt path and the melt path is short during the short path scan, and the total time in the heat-affected zone is longer when the adjacent melt paths are processed near the node, which is conducive to the accumulation of heat. The overall slow cooling time during the cladding period is less for the spiral scan and the long path scan than for the short path scan, and less heat is lost by heat convection and heat radiation, but the temperatures in the short path scan are higher than those in the other paths. This indicates that the use of inter-path air cooling to reduce heat accumulation at the end of each melt path is not significant, and the selection of different scanning paths is more beneficial to reduce heat accumulation during the melting process.

## 4 FE analysis of residual stresses in laser cladding forming

### 4.1 Residual stress distribution at different scan paths

After the temperature field solution was completed, the temperature field loads were read for stress field FE simulation, and Fig. 8 shows the distribution of von Mises stresses using each scanning strategy. It can be seen from the stress cloud diagram that the distribution of stress values shows consistency with the scanning direction of laser cladding, where the temperature gradient between the front end and the back end of the melt pool is large in the scanning direction and the stress values are large, which is consistent with the results of the literature [19, 20]. During the melting and cladding process, transverse cracks are easily induced if the parameters are not selected reasonably. When the first melt layer is formed, the bottom is affected by the shrinkage and deformation, and tensile stresses are generated at the bond between the melt layer and the substrate, while there is only convective heat exchange with the air around the melt layer without other constraints, so the residual stress values of the first melt layer under all four scanning paths are smaller than those of the other melt paths.

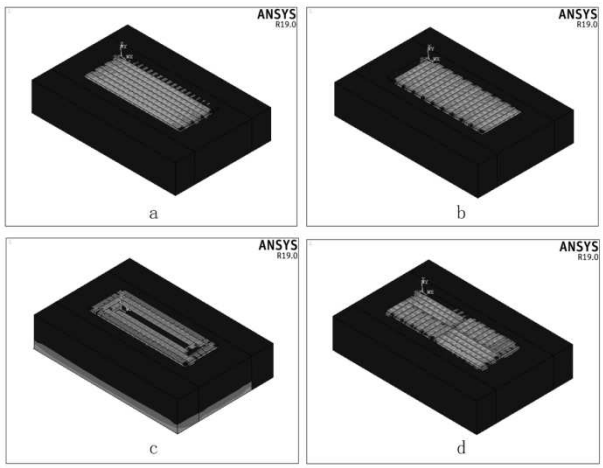


***Fig. 8*** *Cloud of residual stress distribution*

### 4.2 Analysis of the evolution of residual stresses in different paths

In order to study the distribution of residual stress in different directions during the laser cladding process, with reference to the path schematic in Fig. 4, the orientation analysis of the cladding layers of the four scanning strategies is performed separately, defining paths Path1 (along the X-axis direction) and Path2 (along the Z-axis direction). By studying the stress evolution law of the nodes at different locations, stress concentration can be avoided, workpiece deformation can be reduced, and cladding quality can be improved.

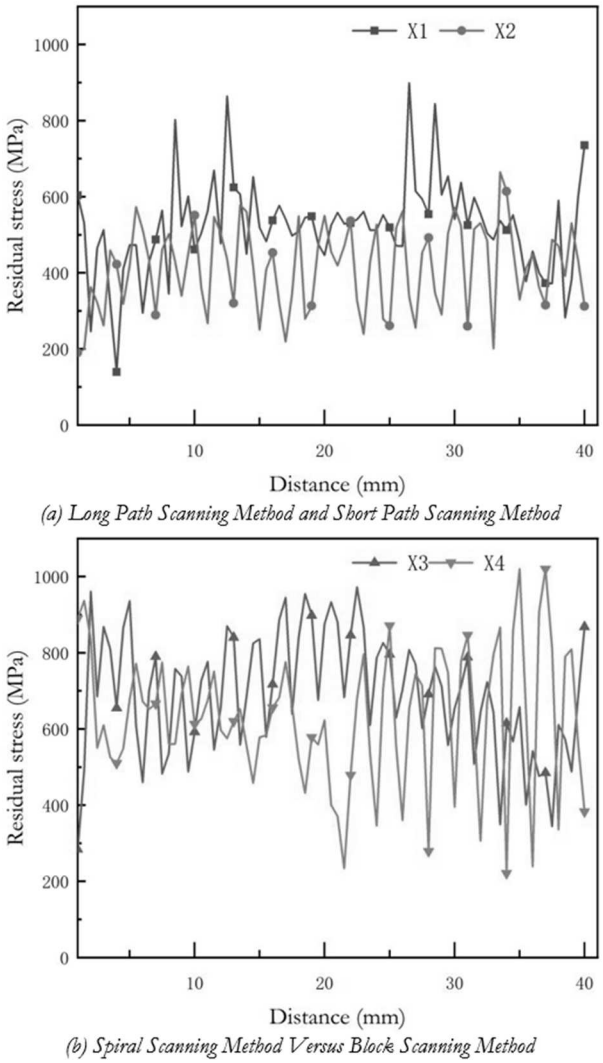


***Fig. 9*** *Node stress cycling along Path1*

As shown in Fig. 9 (a), the stress cycling curves of the nodes along the X-axis direction in the long path scan (X1) and short path scan (X2) methods, the residual stress fluctuation value of the molten layer is more stable after using the short path scan, and the stress value of the molten layer with the long path scan shows an increasing trend at both ends of the molten layer, while the stress value fluctuates smoothly in the middle. This is because during the laser cladding process, after the cladding along the long side, the coating has a long time to cool down. When the next cladding is carried out, the area to be processed is less affected by the heat of the formed area, and the high energy density laser heat source irradiates the surface layer of the substrate, and the temperature of the cladding area climbs sharply causing a large temperature gradient and thermal stress. As the spot moves, the temperature gradient between the substrate and the clad layer gradually decreases, and when the heat input value of laser energy and the heat lost from the substrate reaches a dynamic equilibrium, the stress level is more stable, which is consistent with the trend in the middle of the curve in the figure.

When laser cladding is performed by a short path, the heat generated by the finished coating can preheat the next clad area. After a short period of heat transfer, the temperature of the area to be coated climbs, and the laser operates in this area. The temperature difference during the whole coating process is smaller than that of the long path coating, and the temperature change is smooth so that the deformation variable generated during the slow cooling process is smaller than that of the long path scanning, and the tensile stress generated is smaller.

As shown in Fig. 9 (b), the stress evolution curves of the nodes along the Z-axis for the spiral scanning (X3) and block scanning (X4) methods. The residual stress value of the clad layer is "W" distributed when the spiral scan is used. After the end of the clad layer is formed, the temperature drop is more obvious under the dual effect of heat conduction and convection heat transfer, and the thermal stress is higher than that inside the clad layer. The stress cycling curve is significantly different at the horizontal axis X=20mm when block scanning is used, with a small change in the stress at the left end and a significant change in the stress undulation line at the right end. As the laser coating direction is not consistent in the block scanning, the stress value on the left side of the curve is perpendicular to the scanning direction, and the stress distribution is uniform and fluctuates less throughout the process, while the right side of the curve is parallel to the scanning direction, and the thermal stress changes during the coating process until the temperature of the coating area decreases gradually.

As shown in Fig. 10, the stress cycle curves of the nodes at the bond of the molten layer along the Z-axis direction for each scan path, the short path, and long path scans have approximately the same magnitude of stress cycle curve variation, and the residual stress values obtained along the short side scan are lower than those along the long side scan. The stress values of the spiral scan and the chunked scan showed wave crest and trough variations with approximately the same trend.

The stress data points of the nodes under the above four scanning paths varying along different directions were analyzed for the mean value, and the final results are shown in Fig. 11. The numbers 1, 2, 3, and 4 represent long-path scanning, short-path scanning, spiral scanning, and block scanning. The average residual stress values in the figure show that the short path scanning, whether along the laser scanning direction (406. 68 MPa) or perpendicular to the scanning direction (284. 45 MPa), the residual stress values are smaller than the other scanning methods, and the results are the best. With the short path scanning method, the scanning time interval between adjacent cladding areas is short, which is conducive to heat accumulation, the small temperature difference between cladding layers, smaller shrinkage deformation, and lower tensile stress level. The stress values of 512. 77 MPa and 523. 12 MPa along different directions of the long path scanning method are greater than those of the short path scanning method. The main reason is that when long path scanning, the melting time of each melt path is longer, the heat generated by the melting process has a long time for heat transfer, and the temperature difference between adjacent melting areas is large, which will generate larger residual stresses. The stress values obtained by spiral and block scanning are greater than those obtained by short and long path scanning, because the scanning direction of spiral and block scanning is changing during the melting process, and because the area to be melted is gradually moving away from the melted area, the effect of thermal influence is small, the temperature gradient is higher, the tensile stress is greater, and the residual stress inside the melted layer is larger. Comparing the results of the above analysis, it is finally concluded that the residual stress values under different scanning strategies for single-layer multi-layer laser cladding forming are, from largest to smallest: spiral scanning, block scanning, long path scanning, and short path scanning.

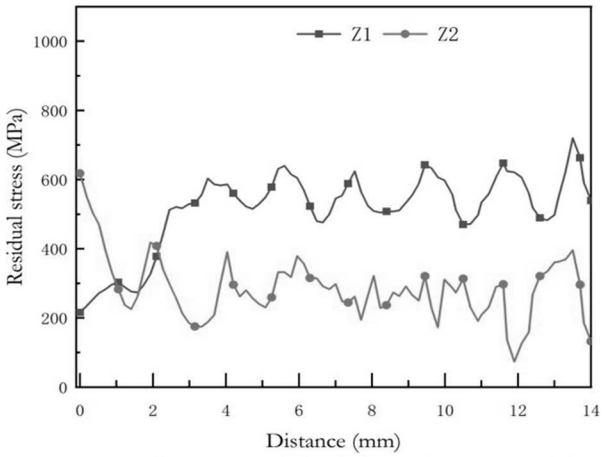


*(a) Long Path Scanning Method and Short Path Scanning Method*

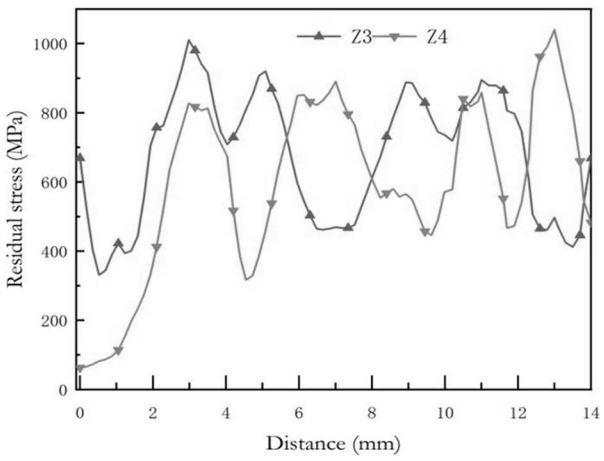


*(b) Spiral Scanning Method and Block Scanning Method*

***Fig. 10*** *Node stress cycling along Path2*

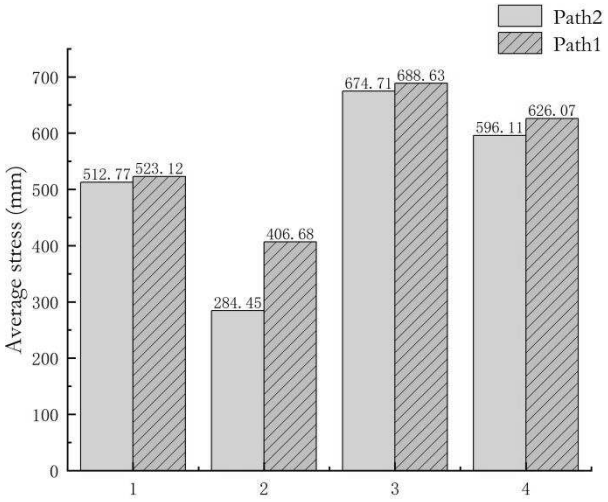


***Fig. 11*** *Histogram of the mean value of nodal stress with path variation*

## 5 Conclusion

The effect of different scanning paths on single-layer multi-path laser cladding forming was analyzed by cladding Ni60A powder on the surface of H13 mold steel, including the melt pool temperature morphology, node change history with temperature, and residual stress evolution law during the cladding process. The results of this study provide theoretical guidance for the selection of paths during cladding processing to reduce the waste of resources and also provide new ideas for exploring the feasibility of metallurgical bonding of materials to substrates, and the specific conclusions are as follows.

- (1) During short path scanning, the short time interval between the adjacent time of melting and cladding is conducive to the accumulation of heat, and the melt pool temperature is higher. In long-path scanning, there is more time to transfer heat to the surrounding medium after melting, and the overall substrate temperature is increased. When spiral scanning, the melting path is gradually expanded from inside to outside, and the priority melting place dissipates heat to the circumference, and the heat transfer is more obvious. In block scanning, the regional continuity is poor, heat dissipation is more and the melt pool temperature is the lowest.
- (2) Four different scanning paths are used for single-layer multi-lane laser cladding tests to extract the morphology of the melt pool at different time points. The temperature of the central node of the melt pool is found to change gradually with time, with three peak changes in temperature at each node, two of which are influenced by the residual heat of the adjacent melting channels, but the temperature values are lower than the melting point of the material and no remelting occurred.
- (3) The residual stress values along the Path1 (X-axis) and Path2 (Z-axis) directions of the four scanning paths are extracted and analyzed, and the stress values of the short path scan are 406.68 MPa and 284.45 MPa, respectively, which are lower than the average values of the other scanning paths in all directions. The residual stress values for different scanning strategies are from largest to smallest: spiral scan, block scan, long path scan, and short path scan.

## Acknowledgement

***This work was financially supported by Science and Technology Project of Jilin Provincial Science and Technology Department of China (20200201220JC); Jilin Provincial Education Department Science and Technology Plan Project (JJKH20220589CY), and authors wish to express their gratitude.***

## References

[1] LI BAN. (2020). H13 Steel Surface Laser Clad Composite Coating and Wear Resistance Study, Yanshan University, China. ISSN 1007-791X.

[2] LI JIANING. (2015). *Laser Cladding Technology and Applications,* pp. 163 - 170. Chemical Industry Publisher, China. ISBN 9787122251336.

[3] LI C, YANG X, WANG S. (2020). Preparation of WC reinforced Co-Based alloy gradient coatings on a H13 mold steel substrate by laser cladding. In: *Coatings*, Vol. 10, No. 2, pp. 176. Korea. ISSN 2079-6412.

[4] REN ZHONGHE, WU MEIPING, TANG YOUHONG. (2019). Numerical simulation and experimental study of laser cladding based on thermodynamic coupling. In: *Advances in Lasers and Optoelectronics*, Vol. 56, No. 5, pp. 176 - 185. China. ISSN 1006-4125.

[5] MA L, ZHANG P, MENG L D. (2011). Finite element calculation of the residual stress and strain of coating during laser cladding process. In: *Journal of Academy of Armored Force Engineering*,

Vol. 2, No. 1, pp. 53 - 59. China. ISSN 1672-1497.

[6] WU YU, MA PENGZHAO, BAI WENQIAN, (2021). Numerical simulation of the temperature field-stress field during laser cladding of 316L/AISI304 with different scanning strategies. In: *Chinese Journal of Lasers*, Vol. 48, No. 22, pp. 18 - 29. China. ISSN 0258-7025.

[7] TAMANNA N, CROUCH R, NAHER S. (2019). Progress in numerical simulation of the laser cladding process. In: *Optics and Lasers in Engineering*, Vol. 122, No. 1, pp. 151 - 163. England. ISSN 0143-8166.

[8] ZHU L, WANG S, PAN H, (2020). Research on remanufacturing strategy for 45 steel gear using H13 steel powder based on laser cladding technology. In: *Journal of Manufacturing Processes*, Vol. 49, pp. 344 - 354. United States. ISSN 0278-6125.

[9] VUNDRU C, PAUL S, SINGH R, (2018). Numerical analysis of multi-layered laser cladding for die repair applications to determine residual stresses and hardness. In: *Procedia Manufacturing*, Vol. 26, pp. 952 - 961. United States. ISSN 1526-6125.

[10] Koreček D, Solfronk P, Sobotka J. (2020). Numerical simulation as a tool to predict sheet metal forming process of TRIP Steel HCT690. In: *Manufacturing Technology*, Vol. 20, No. 5, pp. 625-631. Czech Republic. ISSN 1213-2489.

[11] LIU YANCONG, YI PENG, SHI YONGJUN. (2018). *Laser Cladding Repair Remanufacturing Technology,* pp. 18 - 20. Science Publisher, China. ISBN 9787030567741.

[12] JIA CHANGZHI, HU RENXI, KANG SHIYAN. (2017). *ANSYS 18.0 Thermodynamic Finite Element Analysis from Introduction to Mastery,* pp. 12 - 13. Machinery Industry Publisher, China. ISBN 9787111572237.

[13] PROCHAZKA J, VILIS J, DOBROCKY D, et al. (2023). Modification of diffusion layers by laser shock peening. In: *Manufacturing Technology,* Vol. 22, No. 6, pp. 724 - 732. Czech Republic. ISSN 1213-2489.

[14] DING LIJUAN, CHENG QIYUAN. (2017). *Numerical Calculation Method*, pp. 178 - 179. Higher Education Publisher, China. ISBN 9787040324655.

[15] TIAN MEILING. (2014). *Multi-Layered Stacked Solid Forming and Temperature Field Simulation Study of Optical In-Feed Powder*, SuZhou University, China. ISSN 2095-7068.

[16] YANG G, XIE Y, ZHAO S, et al. (2022). Methods and mechanism of powder mixing for selective laser melting. In: *Manufacturing Technology,* Vol. 22, No. 1, pp. 102-110. Czech Republic. ISSN 1213-2489.

[17] LI MEIYAN, HAN BIN, CAI CHUNBO, (2015). Numerical simulation of the temperature and stress fields of laser clad nickel-based alloys. In: *Journal of Welding*, Vol. 36, No. 5, pp. 25 - 28 + 32 + 114. China. ISSN 0253-360X.

[18] LUO Z, ZHAO Y. (2018). A survey of finite element analysis of temperature and thermal stress fields in powder bed fusion Additive Manufacturing. In: *Additive Manufacturing*, Vol. 21, pp. 318 - 332. Netherlands. ISSN 2214-8604.

[19] LI C, LIU Z Y, FANG X Y. (2018). Residual stress inmetai additive manufacturing. In: *Procedia CIRP*, Vol. 3, pp. 348 - 353. France. ISSN 2212-8271

[20] DENG DEWEI, CHANG ZHANDONG, MA YUNBO, (2021). Effect of process parameters on the tissue properties and residual stresses of 316L laser-clad layers. In: *Application Lasers*, Vol. 41, No. 1, pp. 83 - 88. China. ISSN 1000-372X.